FFI Norwegian Defence Research Establishment

24/01928

FFI-REPORT

Computational fluid dynamics (CFD) modelling of aerodynamic coefficients of projectiles moving at subsonic and supersonic speed

John F. Moxnes
Tallak H. Risdal
Øyvind Grandum
Øyvind Frøyland

Computational fluid dynamics (CFD) modelling of aerodynamic coefficients of projectiles moving at subsonic and supersonic speed

John F. Moxnes
Tallak H. Risdal
Øyvind Grandum
Øyvind Frøyland

Norwegian Defence Research Establishment (FFI) 14 November 2024

Keywords
Ballistikk
Computational Fluid Dynamics (CFD)
Hydrokoder

FFI report
24/01928

Project number
1603

Electronic ISBN
978-82-464-3565-7

Approvers
Hege Jodahl, *Research Manager*
Arne Petter Bartholsen, *Director of Research*

The document is electronically approved and therefore has no handwritten signature.

Summary

Aerodynamic coefficients of drag, lift and overturning moment for a small-calibre projectile are calculated using computational fluid dynamic (CFD) modelling applying the Fluent hydrocode. 250 computational cores were used in a cluster of 1600. The aerodynamic coefficients are well approximated using a third order polynomial in yaw in the subsonic and supersonic regions. A comparison is made with data from the literature. CFD results of drag coefficient agree well with results based on radar measurements.

Generally, CFD seems to provide a basis for significant improvement in projectile accuracy across all calibers of ammunition. It can be argued that this can have large importance for future development of ammunition. Work beyond this report is in progress and has been performed for 120 mm tank ammunition with success theoretically and practically.

Section 2 considers the general theory of projectiles. Section 3 shows analytical theory of aerodynamic coefficients. Section 4 presents results, while Section 5 concludes with discussion.

Sammendrag

Vi har studert de aerodynamiske koeffisientene for drag, løft og tippmoment til et småkaliberprosjektil. Studien er gjort ved strømningssimulering i programmet Fluent. 250 kjerner ble brukt, av et cluster på 1600. Koeffisientene kan tilnærmes godt med tredjeordens polynomer i yaw-vinkel i det subsoniske og det supersoniske området. Vi har gjort en sammenlikning med data fra litteraturen. Beregnet drag stemmer bra med resultater fra radarmålinger.

Det framstår som om CFD-modellering nå kan vise nøyaktighet av alle aerodynamiske koeffisienter til prosjektiler. Dette gir grunnlag for betydelig forbedring i prosjektilnøyaktighet, på tvers av alle kalibre fra 5,56 mm til 155 mm. Det kan hevdes at dette vil ha stor betydning for utvikling av forbedret ammunisjon. Arbeid utover denne rapporten pågår.

Del 2 betrakter den generelle teorien om prosjektiler. Del 3 viser analytisk teori om aerodynamiske koeffisienter. Del 4 viser resultater, mens del 5 avsluttes med diskusjon.

Contents

1 Introduction

Inverse modelling of radar tracking data gives valuable insight into drag and spin of projectiles. Spark range measurement may outline structure of lift, overturning moment, Magnus, and pitch damping coefficients (Silton and Weinacht 2008). PRODAS (PRODAS 2000) uses a database of parameters (coefficients) for projectiles constructed of segments of frustums. However, the coefficients are difficult to validate by experimental methods and by wind tunnel measurements.

CFD modelling has been used to establish drag (Danaberg and Nietubicz, 1992, Sahu and Heavey 1996, Dietrich et al. 2004, Silton and Weinacht 2008, Suliman et al. 2009). The modelling has also been used to validate stability of spinning projectiles (Cayzac et al. 2004).

A turbulent boundary layer separates at the base corner of a projectile during flight. A low-pressure region is formed immediately downstream of the base, which is characterized by a low velocity recirculation region. Interaction between this recirculation flow and the inviscid external flow occurs through free shear mixing which gives turbulent flow. However, turbulent flow is difficult to model. The RANS (Reynolds Averaged Navier-Stokes) models have low computational cost and reasonable accuracy. In this report, the k-omega SST (Shear-stress transport) model is used. The model is the blending of the standard k-epsilon model that is suitable for a shear layer problem, and the Wilcox k-omega model that is suitable for wall turbulence effects. K-omega SST has shown good quality for compressible flow (Sharif and Guo 2007). Detached eddy simulation (DES) has been used in the literature (Kubberud and Øye 2011, Zhang et al. 2008). DES requires an unsteady flow solver and statistical averages of the computed flow fields to extract the average forces.

CFD modelling by hydrocodes may now show accuracy of all aerodynamic coefficients of projectiles. This provides the basis for significant improvement in projectile accuracy across all calibres from 5.56 mm to 155 mm. It can be argued that this can have large importance for development of improved ammunition, and work beyond this report is in progress.

Section 2 outlines the general theory of projectiles. Section 3 shows analytic theory of aerodynamic coefficients. Section 4 show results, while section 5 concludes with some discussion.

2 General theory

The drag force is given as

$$\vec{F}_D = -\frac{1}{2}\rho S C_D V^2 \vec{i}, \quad \left\|\vec{F}_D\right\| = \frac{1}{2}\rho S C_D V^2 \tag{2.1}$$

where $\vec{V}$ is the velocity of the centre of mass of the projectile, $\left\|\vec{V}\right\| = V$, and $\vec{i} = \vec{V} / \left\|\vec{V}\right\|$ is the unit velocity vector of the centre of mass. *S* is the projected area of the projectile on the surface with normal vector along the projectile axis. ρ is the air density, while C_D is the drag coefficient.

The lift force $\vec{F}_L$ is given as

$$\vec{F}_L = \frac{1}{2}\rho S C_{L_\alpha} V^2 \left(\vec{i} \times (\vec{x} \times \vec{i})\right), \quad \left\|\vec{F}_L\right\| = \frac{1}{2}\rho S C_{L_\alpha} V^2 \sin\alpha \tag{2.2}$$

where $\vec{x}$ is the unit vector along the projectile geometric axis. C_{L_α} is the lift coefficient derivative, while α is the angle of attack (yaw angle) defined by

$$\alpha \equiv \arccos(\vec{i} \cdot \vec{x}) \tag{2.3}$$

Thus

$$\cos\alpha = (\vec{i} \cdot \vec{x}), \quad \sin\alpha = \sqrt{1-\cos^2\alpha} = \sqrt{1-(\vec{i} \cdot \vec{x})^2} \tag{2.4}$$

The lift and drag give torque (force moment) on the projectile. The overturning moment is

$$\vec{M}_\alpha = -\frac{1}{2}\rho S d C_{M_\alpha} V^2 (\vec{x} \times \vec{i}), \quad \left\|\vec{M}_\alpha\right\| = \frac{1}{2}\rho S d C_{M_\alpha} V^2 \sin\alpha \tag{2.5}$$

where *d* is the diameter of the projectile and C_{M_α} is the overturning moment coefficient derivative.

3 Analytic theory of coefficients

3.1 Drag coefficient

The *x*-axis in Fluent is along the projectile geometrical axis with the nose in the positive direction. Thus, the air moves in the negative *x*-direction. During yaw, the velocity of air is oblique to the geometric axis of the projectile. The force in *x*-direction is negative, while the force in the *y*-direction is positive.

The drag force is

$$\left\|\vec{F}_D\right\| = \frac{1}{2}\rho S C_D V^2 = -F_x \cos\alpha + F_y \sin\alpha \tag{3.1}$$

where F_x is the force on the projectile along the projectile axis, and F_y is the normal force on the projectile. These two forces give a torque (force moment) M_z on the projectile.

The forces are scaled (normalized) by

$$f_x \equiv \frac{F_x}{\frac{1}{2}\rho S V^2}, \quad f_y \equiv \frac{F_y}{\frac{1}{2}\rho S V^2} \tag{3.2}$$

This gives

$$C_D = -f_x \cos\alpha + f_y \sin\alpha \tag{3.3}$$

3.2 Lift coefficient

The lift force is

$$\left\|\vec{F}_L\right\| = \frac{1}{2}\rho S C_{L_\alpha} V^2 \sin\alpha = F_x \sin\alpha + F_y \cos\alpha \tag{3.4}$$

This gives

$$C_L \equiv C_{L_\alpha} \sin\alpha = f_x \sin\alpha + f_y \cos\alpha \tag{3.5}$$

where C_L is the lift coefficient. The inverse relation gives

$$f_x = -C_D \cos\alpha + C_L \sin\alpha, \quad f_y = C_D \sin\alpha + C_L \cos\alpha \tag{3.6}$$

3.3 Overturning moment coefficient

The lift and drag force give torque (force moment) on the projectile, to read

$$\left\| \vec{M}_\alpha \right\| = \frac{1}{2} \rho S d C_{M_\alpha} V^2 \sin\alpha = M_z \tag{3.7}$$

The torque is scaled (normalized) by

$$C_M \equiv C_{M_\alpha} \sin(\alpha) = \frac{M_z}{\frac{1}{2}\rho S d V^2} \tag{3.8}$$

where C_M is the overturning moment coefficient.

The following values are used in the simulations:

$$c = 347.09\,\text{m/s},\ \rho = 1.177\,\text{kg/m}^3,\ d = 0.00782\,\text{m},\ S = \pi(d/2)^2 = 4.8029\,10^{-5}\,\text{m}^2 \tag{3.9}$$

where c is the speed of sound.

See Appendix A for details on the computational method using Fluent for the projectile NM258, and Appendix B for details on radar tracking for NM258.

4 Results

4.1 Drag, lift and overturning moment coefficients

Fluent simulations are applied at different yaw angles up to 13°. The Mach numbers (*M*) are 0.5, 0.7, 0.8, 0.9, 1.09, 1.15, 1.3, 1.5, and 2.0. See Appendix A for simulation details. For each yaw angle and Mach number the numerical values for forces F_x, F_y, and torque M_z are derived from Fluent. The data are transformed to data for drag coefficient C_D, lift coefficient C_L, and overturning moment coefficient C_M. For every Mach number *M* a least squares regression fit (LSF) to the data is chosen. According to the ballistics literature, the following mathematical form should be chosen:

$$\begin{aligned} C_D &= C_{D_0} + C_{D_{\alpha^2}} \sin^2\alpha \\ C_L &= C_{L_{\alpha^1}} \sin\alpha + C_{L_{\alpha^3}} \sin^3\alpha \\ C_M &= C_{M_{\alpha^1}} \sin\alpha + C_{M_{\alpha^3}} \sin^3\alpha \end{aligned} \tag{4.1}$$

For simplicity the subscript "α" is suppressed in this report and we simply write C_{D_0}, C_{D_2}, C_{L_1}, C_{L_3}, and C_{M_1}, C_{M_3}. Moreover

$$C_{L_\alpha} \equiv \frac{C_L}{\sin\alpha} = C_{L_1} + C_{L_3}\sin^2\alpha, \quad C_{M_\alpha} \equiv \frac{C_M}{\sin\alpha} = C_{M_1} + C_{M_3}\sin^2\alpha \tag{4.2}$$

The normalized forces become

$$\begin{aligned} f_x &= -C_D\cos\alpha + C_L\sin\alpha \\ &= -\left(C_{D_0} + C_{D_2}\sin^2\alpha\right)\cos\alpha + \left(C_{L_1}\sin\alpha + C_{L_3}\sin^3\alpha\right)\sin\alpha \\ f_y &= C_D\sin\alpha + C_L\cos\alpha \\ &= \left(C_{D_0} + C_{D_2}\sin^2\alpha\right)\sin\alpha + \left(C_{L_1}\sin\alpha + C_{L_3}\sin^3\alpha\right)\cos\alpha \end{aligned} \tag{4.3}$$

This gives

$$f_x = -C_{D_0} + \left(-C_{D_2} + \frac{1}{2} C_{D_0} + C_{L_1} \right) \sin^2 \alpha + O\left(\sin^4 \alpha \right)$$
$$f_y = \left(C_{D_0} + C_{L_1} \right) \sin \alpha + \left(C_{D_2} + C_{L_3} - \frac{1}{2} C_{L_1} \right) \sin^3 \alpha + O\left(\sin^5 \alpha \right) \tag{4.4}$$

4.1.1 Drag coefficient

Figure 4.1 shows the Fluent results for the drag coefficient together with the least squares fits (LSFs) which are quite good. The transonic region, where M = 0.90 (orange) and M = 0.95 (yellow), deviates somewhat from the regression curve. This may be due to physical conditions where the polynomial development is not satisfactory, or it may be that the turbulence model or the numerical algorithm in Fluent is inappropriate. This has not been investigated further in this report.

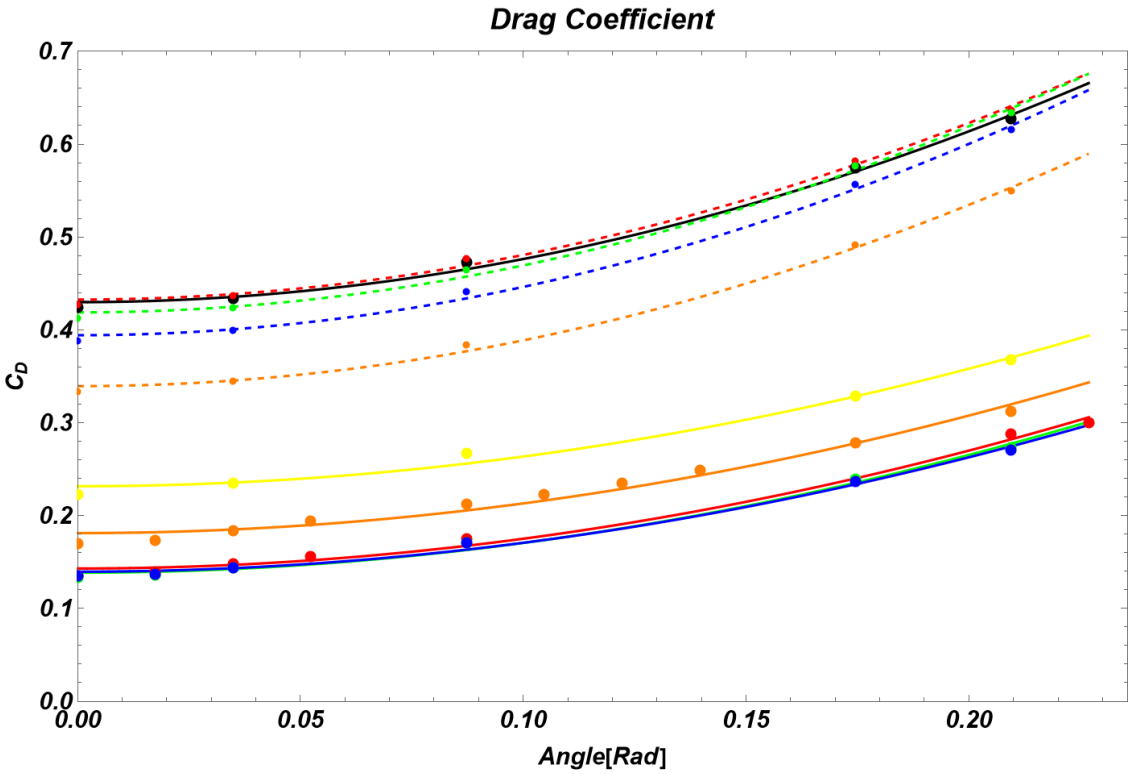

Figure 4.1 The drag coefficient C_D vs yaw for different Mach numbers. Red: M=0.5, Green: M=0.7, Blue: M=0.8, Orange: M=0.9, Yellow: M=0.95, Black: M=1.09, Red dashed: M=1.15, Green dashed: M=1.30, Blue dashed: M=1.50, Orange dashed: M=2.00. Data points are from Fluent. Curves are based on LSF.

4.1.2 Lift coefficient

Figure 4.2 shows the Fluent results for the lift coefficient together with the LSFs which are quite good. Again, deviations are seen for $M = 0.90$ and $M = 0.95$. It is observed that the curvature is negative subsonic and positive supersonic.

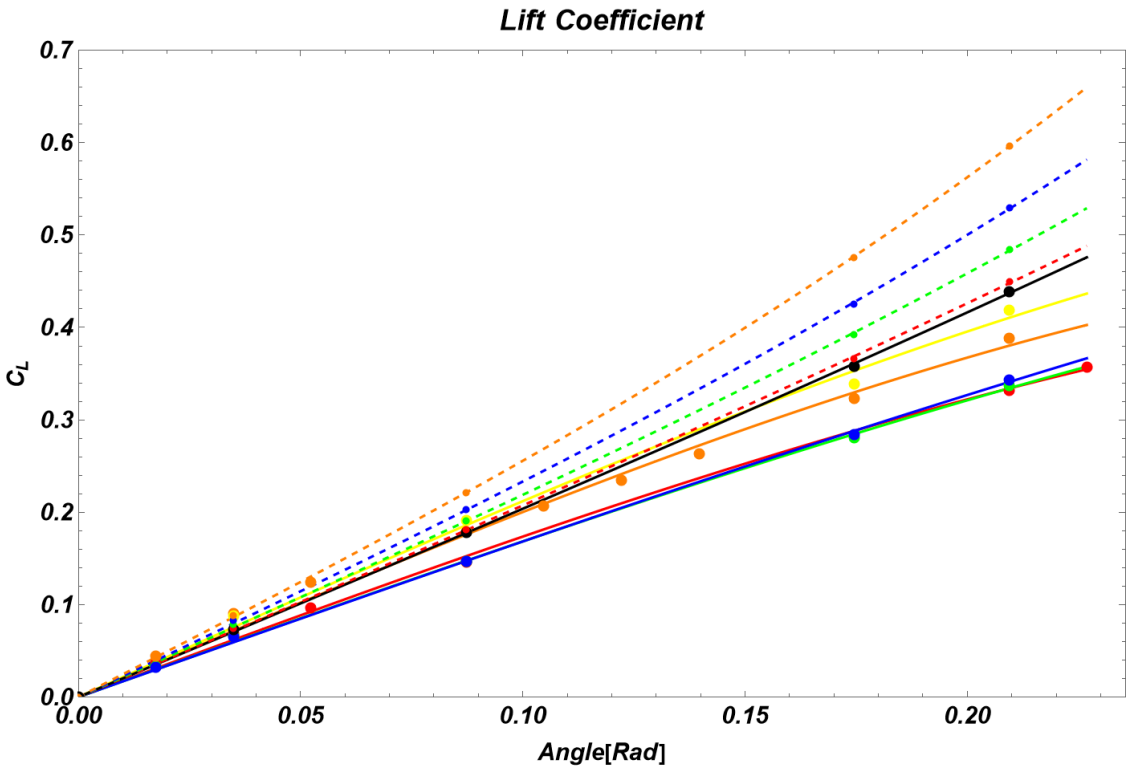

Figure 4.2 The lift coefficient C_L vs yaw for different Mach numbers. Red: M=0.5, Green: M=0.7, Blue: M=0.8, Orange: M=0.9, Yellow: M=0.95, Black: M=1.09, Red dashed: M=1.15, Green dashed: M=1.30, Blue dashed: M=1.50, Orange dashed: M=2.00. Data points are from Fluent. Curves are based on LSF.

4.1.3 Overturning moment coefficient

Figure 4.3 shows the Fluent results for the overturning moment coefficient together with the LSFs, which are quite good. The curvature is not very large, but positive subsonic and negative supersonic.

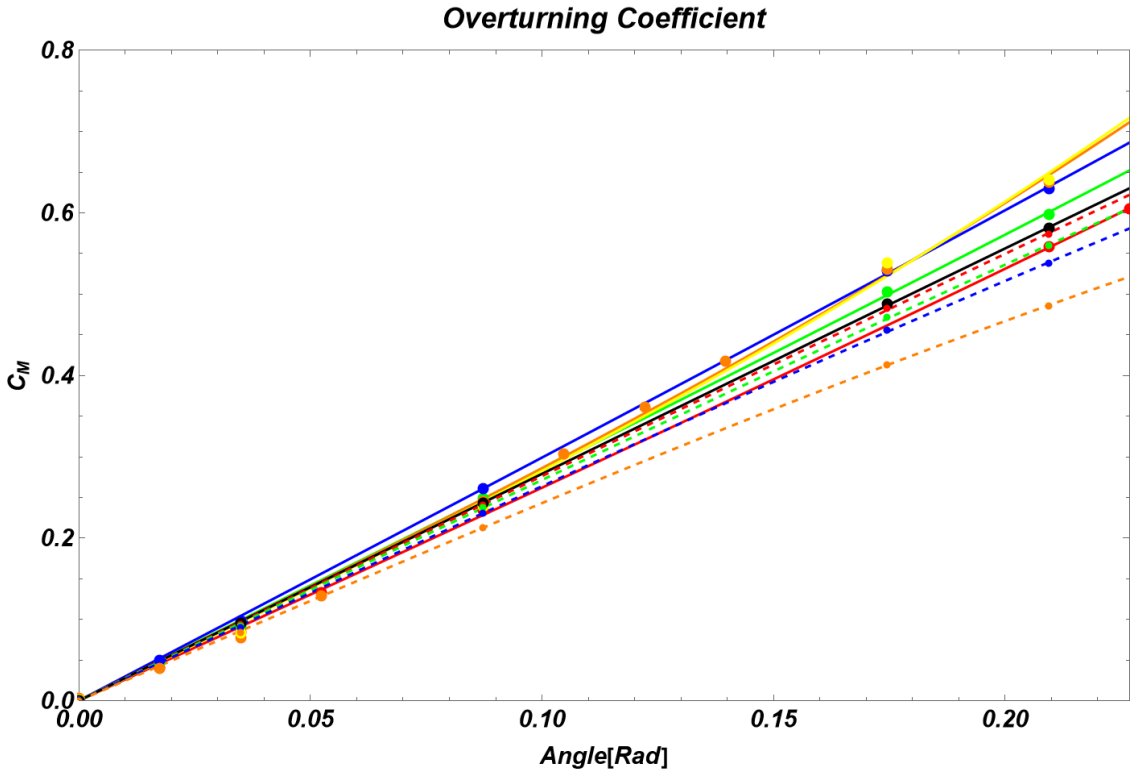

Figure 4.3 The overturning moment coefficient C_M vs yaw for different Mach numbers. Red: M=0.5, Green: M=0.7, Blue: M=0.8, Orange: M=0.9, Yellow: M=0.95, Black: M=1.09, Red dashed: M=1.15, Green dashed: M=1.30, Blue dashed: M=1.50, Orange dashed: M=2.00. Data points are from Fluent. Curves are based on LSF.

4.2 Lift and overturning moment coefficient derivative

The lift and overturning moment coefficient derivatives are often shown in the literature. Figure 4.4 shows the lift coefficient derivative, while Figure 4.5 shows the overturning moment coefficient derivative. The lift coefficient derivative shows negative curvature in the subsonic region, while it is positive in the supersonic region. The absolute value of the curvature is increasing for decreasing Mach numbers in the subsonic region, while it is increasing for increasing Mach numbers in the supersonic region.

The overturning moment coefficient derivative shows positive curvature in the subsonic region, while it is negative in the supersonic regime. The absolute value of the curvature is increasing for decreasing Mach numbers in the subsonic region, while it is increasing for increasing Mach numbers in the supersonic region.

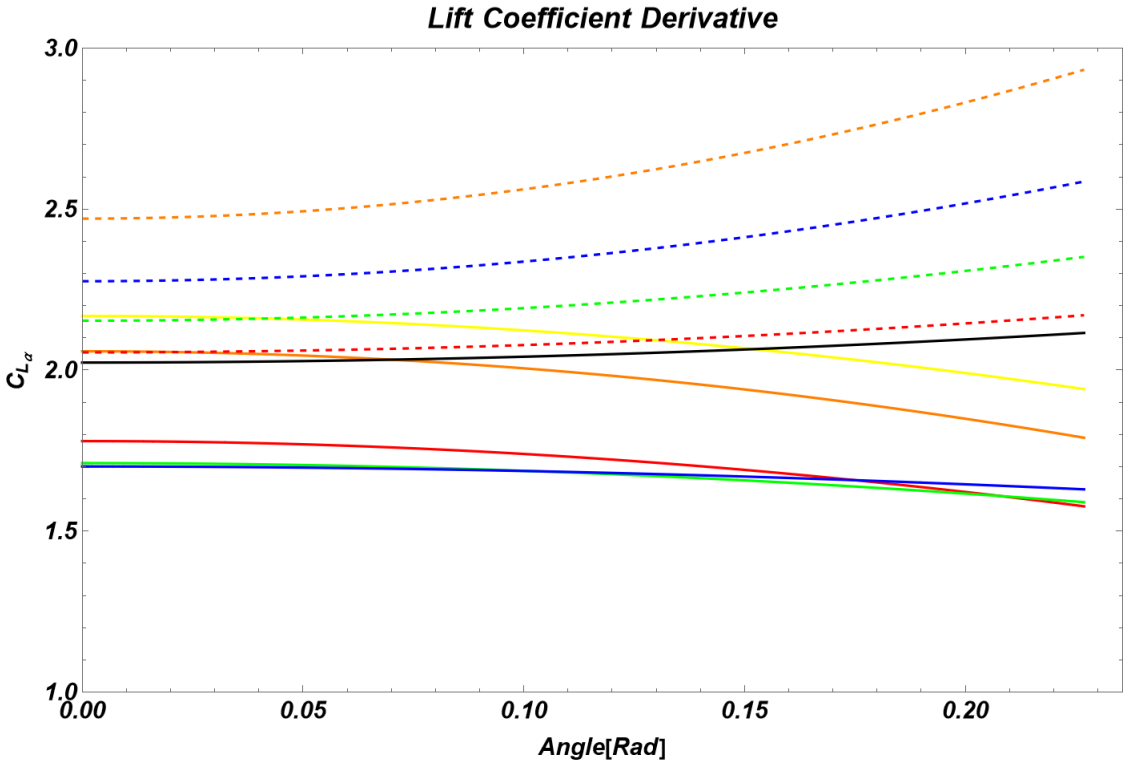

Figure 4.4 The lift coefficient derivative C_{L_α} vs yaw for different Mach numbers. Red: M=0.5, Green: M=0.7, Blue: M=0.8, Orange: M=0.9, Yellow M= 0.95, Black: M=1.09, Red dashed: M=1.15, Green dashed: M=1.30, Blue dashed: M=1.50, Orange dashed: M=2.00.

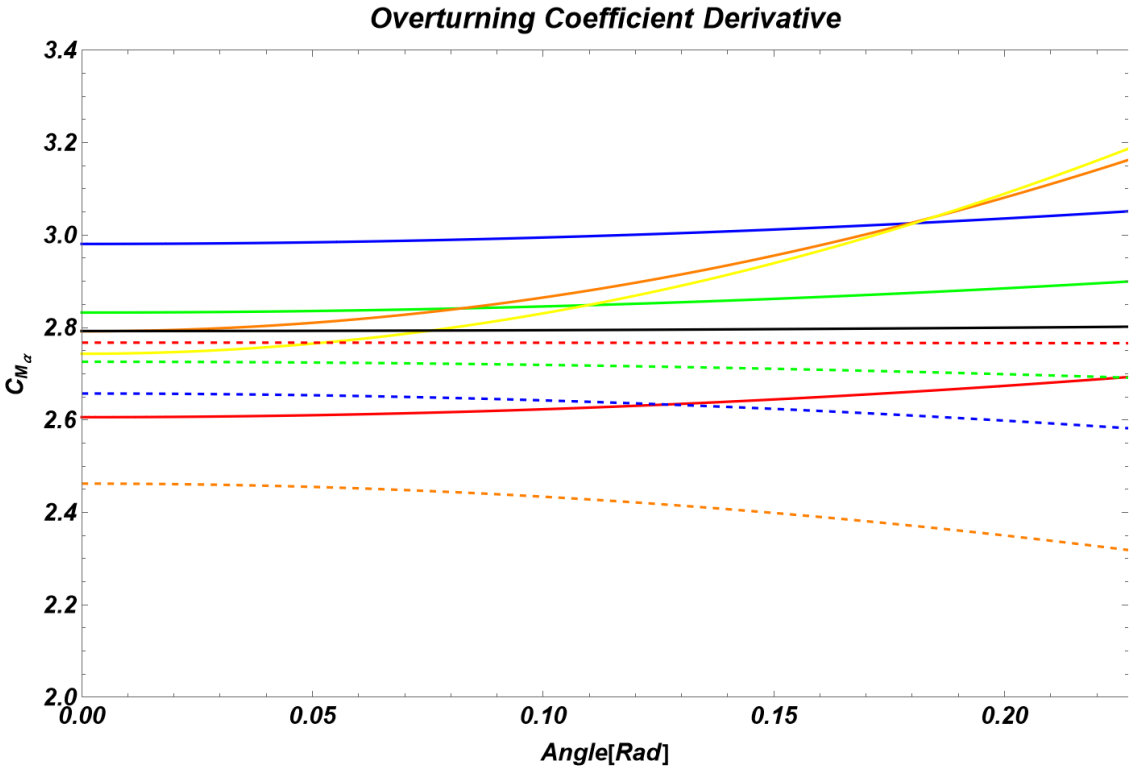

Figure 4.5 The overturning moment coefficient derivative C_{M_α} vs yaw for different Mach numbers. Red: M=0.5, Green: M=0.7, Blue: M=0.8, Orange: M=0.9, Yellow: M=0.95, Black: M=1.09, Red dashed: M=1.15, Green dashed: M=1.30, Blue dashed: M=1.50, Orange dashed: M=2.00.

4.3 Comparing drag, lift and overturning moment coefficients with PRODAS and measurements

PRODAS delivers values for different aerodynamics coefficients. These values were compared with Fluent results and measurements. Figure 4.6 shows C_{D_0} as a function of Mach number. The PRODAS drag coefficient is significantly smaller than Fluent in the supersonic region.

Also shown in Figure 4.6 are the drag coefficients in the literature for 7.62 mm M118 US projectile (McCoy 1985 and 1988). M118 results situate between Fluent and PRODAS. Results for our 7.62 mm NM258 projectile based on inverse modelling of radar data are also shown. NM258 results are slightly below the Fluent results supersonic. Note that the drag coefficient for NM258 deviates from Fluent in the transonic region. This may suggest that the projectile is developing yaw so that a second-order term must be included when applying inverse modelling to establish C_{D_0} from the radar data.

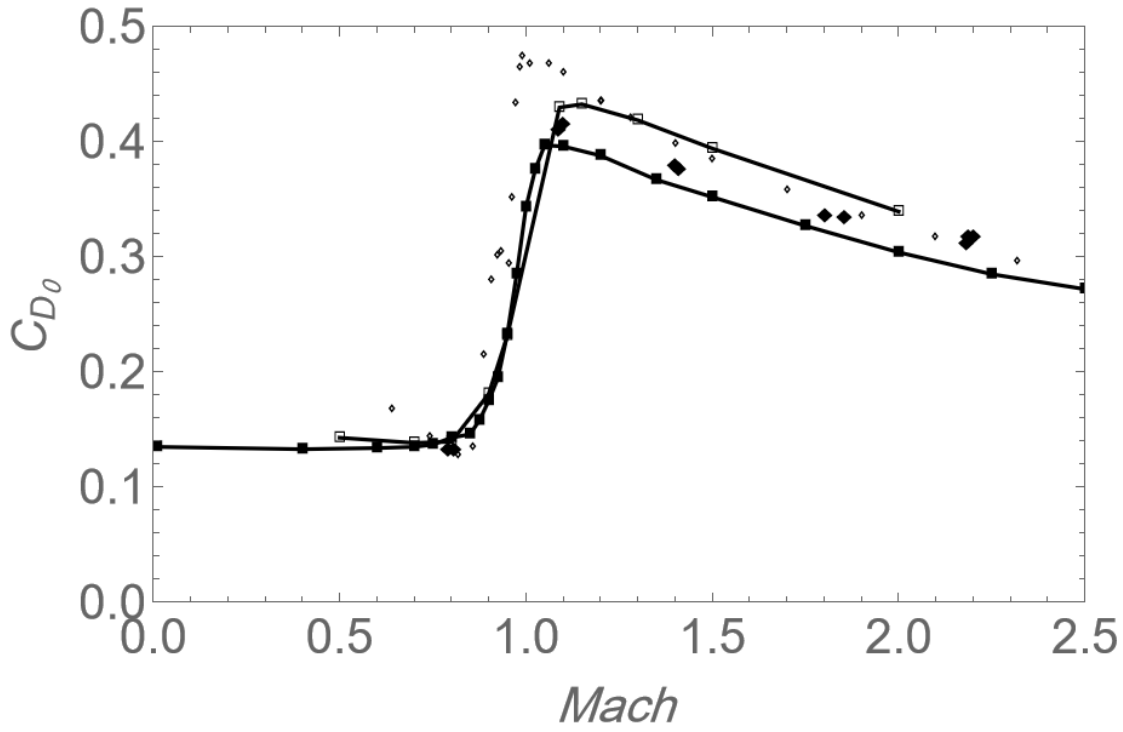

Figure 4.6 The drag coefficient C_{D_0} as a function of the Mach number. Open Square: Fluent, Filled Square: PRODAS, Filled Diamond: Data in the literature for M118, Open Diamond: Radar data for NM258.

Figure 4.7 shows the C_{D_2} drag coefficient as function of the Mach number. Fluent results are smaller than PRODAS. This in contrast to C_{D_0} which is larger for Fluent in the supersonic region. Fluent displays a local maximum above $M = 1$. Here it can be noted that the transonic region does not prove to be problematic in Fluent.

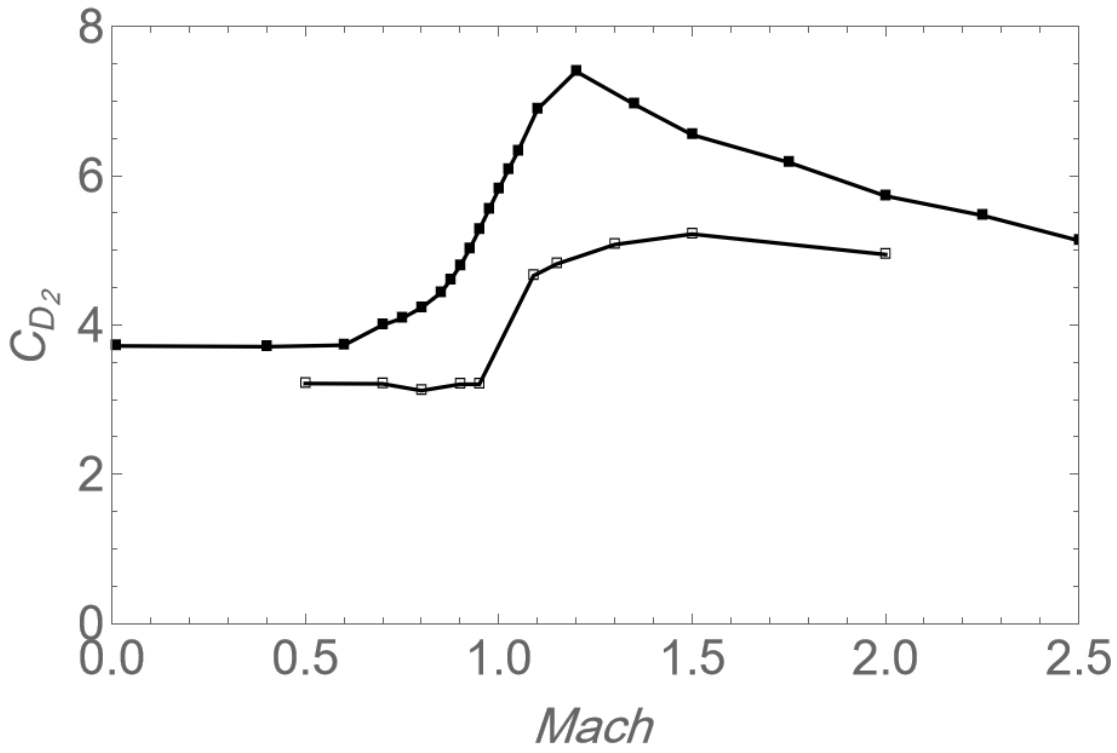

Figure 4.7 The C_{D_2} drag coefficient as a function of the Mach number. Open Square: Fluent, filled Square: PRODAS.

Figure 4.8 shows the C_{L_1} lift coefficient as a function of Mach number. The PRODAS results situate somewhat below Fluent. However, the main structure of PRODAS and Fluent is the same. A local maximum occurs close but on the lower side of $M = 1$, while a local minimum occurs close to and at the upper side of $M = 1$. The M118 results situate both above and below PRODAS and Fluent results. It appears that the transonic region shows the greatest deviation from Fluent and PRODAS.

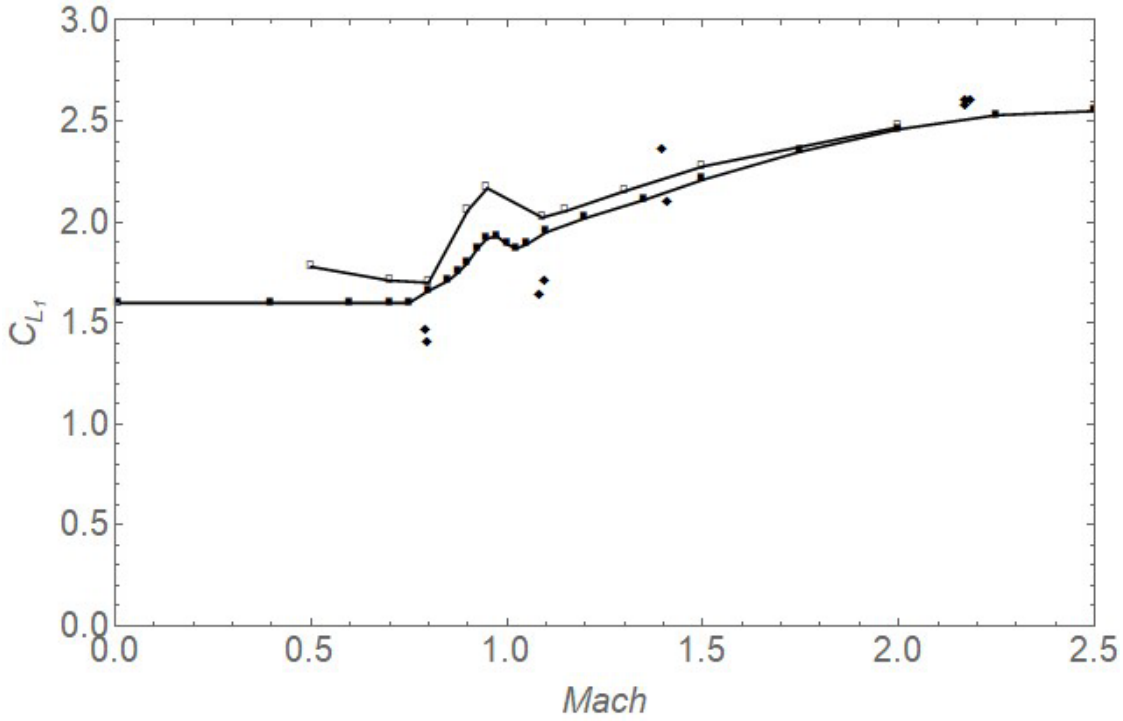

Figure 4.8 The lift coefficient C_{L_1} as a function of the Mach number. Open Square: Fluent, Filled Square: PRODAS, Filled Diamond: M118.

Figure 4.9 shows the results for C_{L_3}. Here a clear difference between Fluent and PRODAS is observed. In the transonic region, where $M = 0.90$ and $M = 0.95$, Fluent shows a local minimum. PRODAS also shows a local minimum, but around $M = 1.2$. Fluent shows a much greater variability than PRODAS. Overall, Fluent shows a coefficient increasing with increasing Mach number, negative in the subsonic region while positive in the supersonic region. PRODAS is negative for all Mach numbers. In PRODAS, the normalized force f_y is approximated linear in $\sin(\alpha)$. This gives according to equation (4.4)

$$C_{D_2} + C_{L_3} - \frac{1}{2}C_{L_1} = 0 \quad \Rightarrow \quad C_{L_3} = \frac{1}{2}C_{L_1} - C_{D_2} \tag{4.5}$$

However, this seems to be a rather bad approximation as Fluent in Figure 4.10 shows significant non-linearity in the supersonic region.

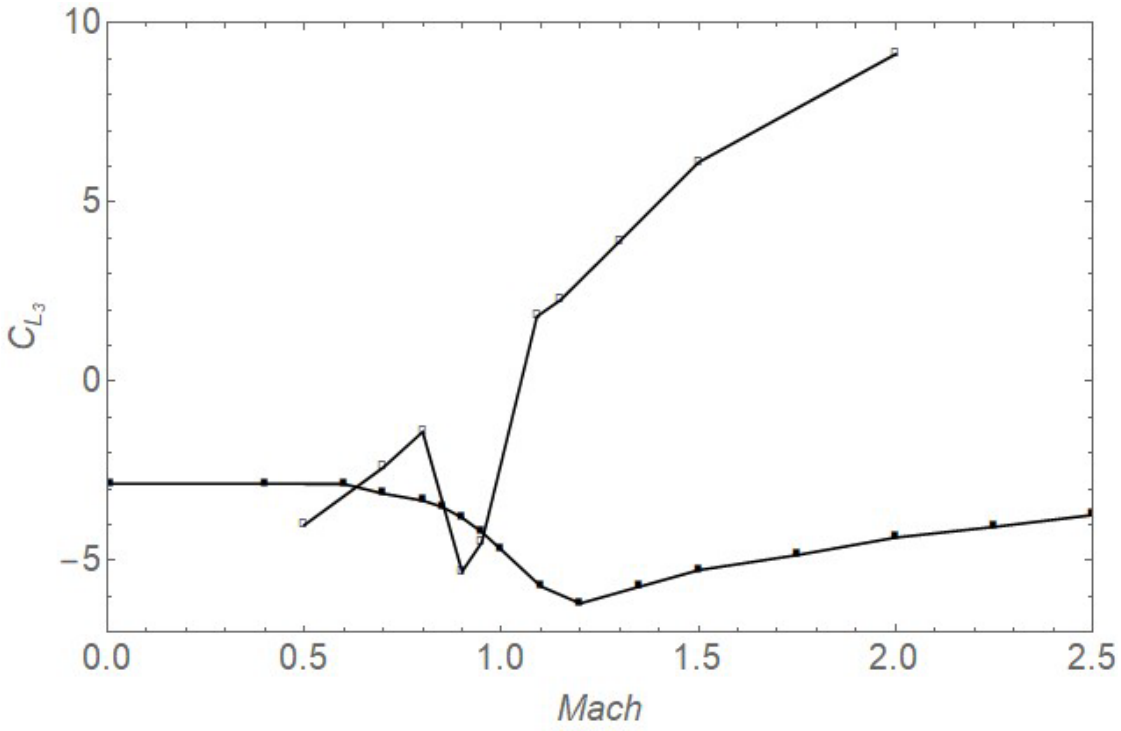

Figure 4.9 The lift coefficient C_{L_3} as a function of the Mach number. Open Square: Fluent, Filled Square: PRODAS.

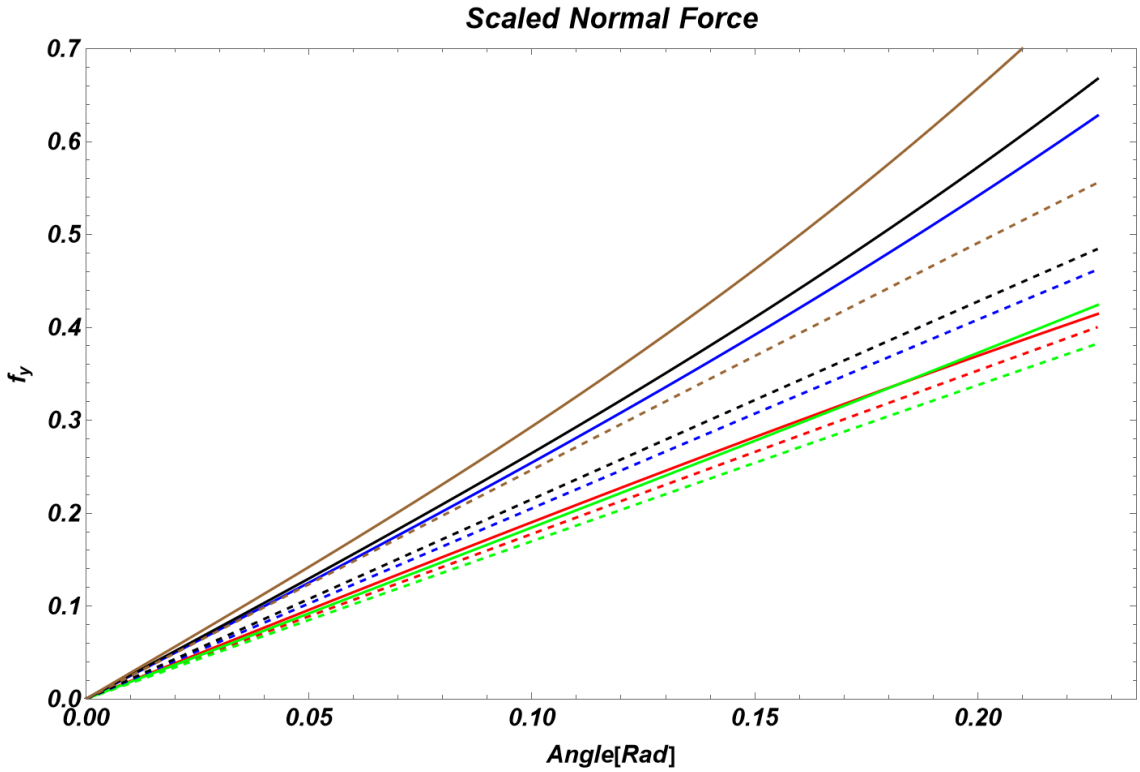

Figure 4.10 The scaled normal force vs yaw for different Mach numbers. Dashed lines are PRODAS approximations. Solid lines are Fluent results. Red: M=0.5, Green: M=0.8, Blue: M=1.15, Black: M= 1.30, Brown: M=2.00.

Figure 4.11 shows the results for C_{M_1}. Both Fluent and PRODAS show two local maxima, one subsonic and one supersonic. The maximum subsonic is shifted to smaller Mach number for Fluent. The local maximum above $M = 1$ is less clear for Fluent. The M118 results situate significantly above PRODAS and Fluent and the coefficient decreases for increasing Mach numbers. This is in contrast to Fluent and PRODAS that show increasing coefficient for increasing Mach numbers in parts of the subsonic and transonic regions.

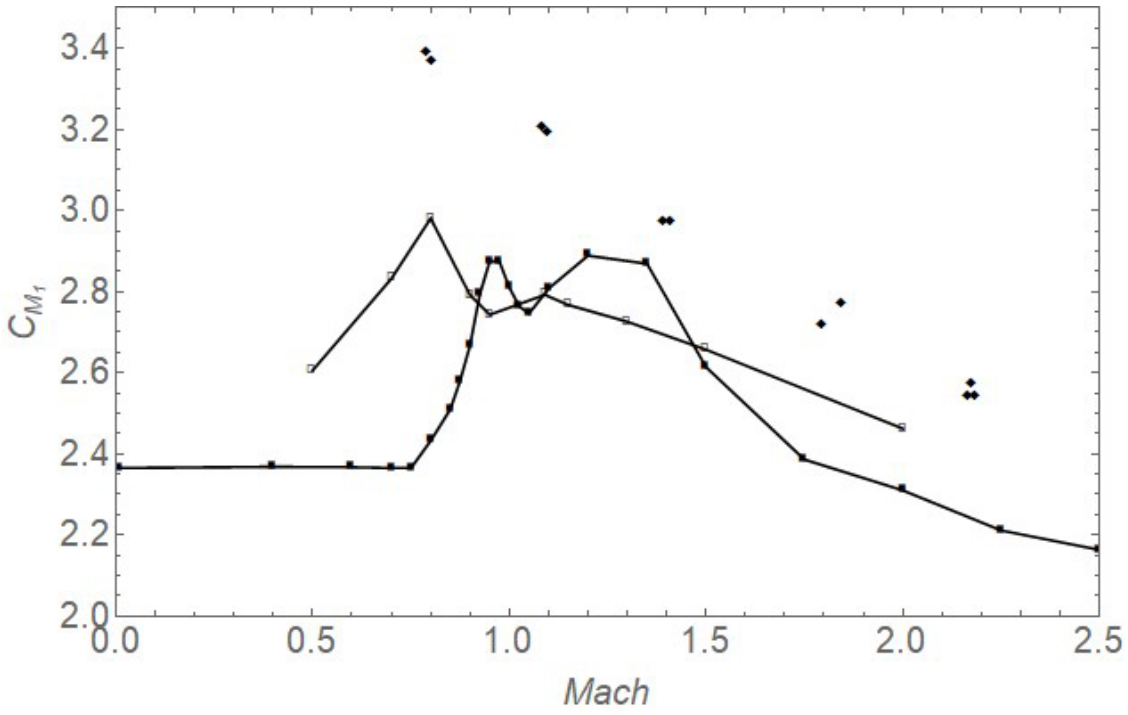

Figure 4.11 The overturning moment coefficient C_{M_1} as a function of the Mach number. Open Square: Fluent, Filled Square: PRODAS, Filled Diamond:M118.

Figure 4.12 shows the results for C_{M_3} . PRODAS does not deliver any value. Fluent shows a local maximum in the transonic region. The overall trend is that the coefficient decreases with increasing Mach number, positive in the subsonic region and negative in the supersonic region.

The radar data of the 7.62 mm NM258 projectile shows elevated drag coefficient in the transonic region. Fluent shows strongly positive and increasing C_{M_3} in the transonic region. This may lead to increased yaw and increased drag on the projectile, which possibly may explain the radar observation. However, 6-DOF models applying the developed C_{M_3} in Fluent does not support this since the influence of C_{M_3} becomes negligible.

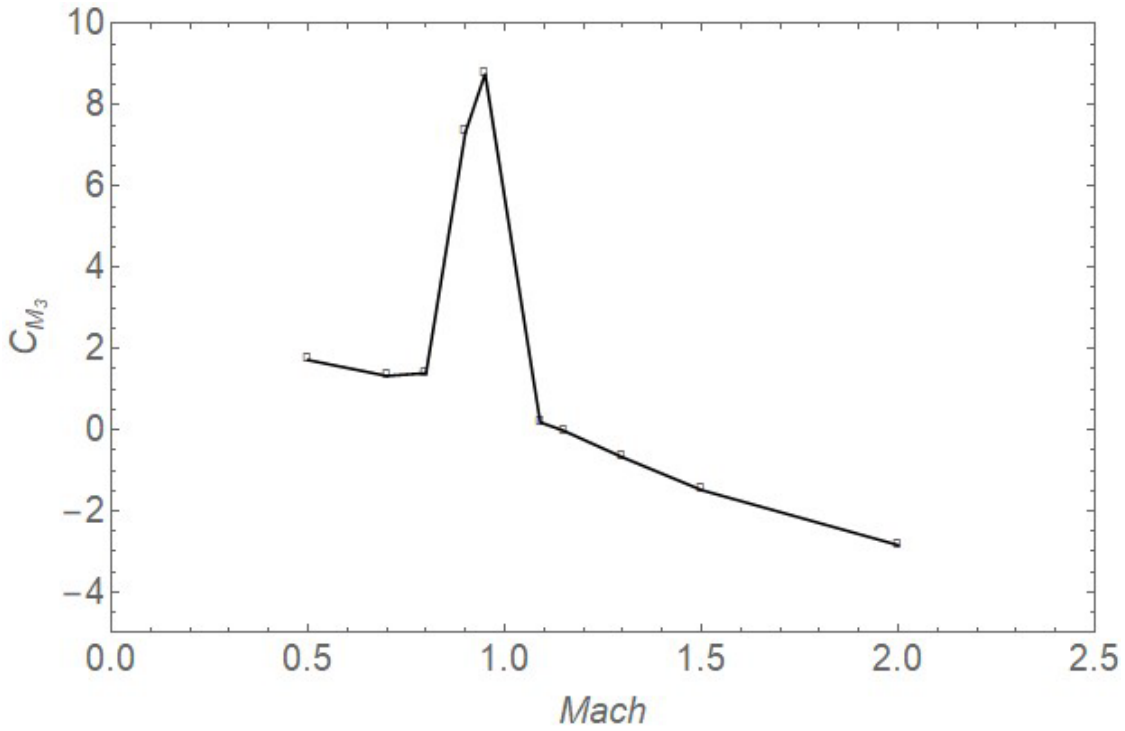

Figure 4.12 The overturning moment coefficient C_{M_3} as a function of the Mach number. Open Square: Fluent.

5 Conclusion and discussion

Aerodynamic coefficients of drag, lift and overturning moment for a small-calibre projectile were calculated using computational fluid dynamic (CFD) modelling applying the Fluent hydrodynamic code. The aerodynamic coefficients were well approximated using a third order polynomial in yaw angle in the subsonic and supersonic region. However, the transonic region shows signs of deviation from the chosen polynomial expansion.

The aerodynamic coefficients calculated using CFD deviate from PRODAS. In particular for the third order coefficient for lift. The reason is that PRODAS assumes the normal force on the projectile to be linear in sinus of the yaw angle. Fluent shows that this approximation is bad in the supersonic region. Third order coefficient for overturning is not tabulated in PRODAS, and a comparison with Fluent can thus not be made.

The radar data of the 7.62 mm NM258 projectile shows elevated drag coefficient in the transonic region. Fluent shows strongly positive and increasing C_{M_3} in the transonic region. This may lead to increased yaw and increased drag on the projectile, which possibly could have explained the radar observation. However, 6-DOF models applying the developed C_{M_3} in Fluent does not support this since the influence of C_{M_3} on yaw becomes negligible. Alternatively, Magnus moment may be an explanation. It is notable that the RANS methodology earlier has been shown to be inappropriate in Magnus prediction in subsonic and transonic region (Simon et al. 2007). The Fluent transonic results for C_{M_3} and C_{L_3} need more research.

Calculations not shown in this report make visible that LSF improves somewhat if one allows the polynomial development to also include a first order term in the drag coefficient, as well as second order terms in the lift and overturning moment coefficient. However, such terms will be inconsistent with the classical ballistics' literature, and we have therefore, for the time being, decided not to include these terms in this study.

Generally, CFD seems to provide a basis for significant improvement in projectile accuracy across all calibres of ammunition. It can be argued that this can have large importance for future development of ammunition. Work beyond this report is in progress and has been performed for 120 mm tank ammunition with success theoretically and practically.

Appendix

A Computational approach

Ansys Fluent has been used for steady state simulations of the flow around the projectile NM258 (see Figure A.1). Turbulence is modelled with the k-omega SST turbulence model. All simulations have been done with Fluent's coupled solver.

A "wind tunnel" is created by making a cylindrical enclosure around the projectile in Ansys SpaceClaim, and the wind tunnel is meshed with Ansys Meshing. The diameter of the wind tunnel is 19.3 times the projectile diameter and the length is 6.8 times the length of the projectile. The projectile surface is covered by an inflation with a first layer depth of $2 \cdot 10^{-7}$ m and a growth rate of 1.2 to ensure a low y+ value. The projectile surface has a maximum element size of 0.225 mm. The volume surrounding the projectile including shock waves and wake has a maximum element size of 0.5 mm, while the rest of the wind tunnel has a maximum element size of 2.5 mm, see Figure A.2. The total number of elements is approximately 113 million. Simulations are performed without spin on the projectile, but with rifling.

Figure A.1 Model of the 7.62 mm NM258 projectile. The geometry (except the rifles) is based on measurements of an unfired specimen. The depth of the rifles was measured on a specimen that was fired from an HK417 rifle.

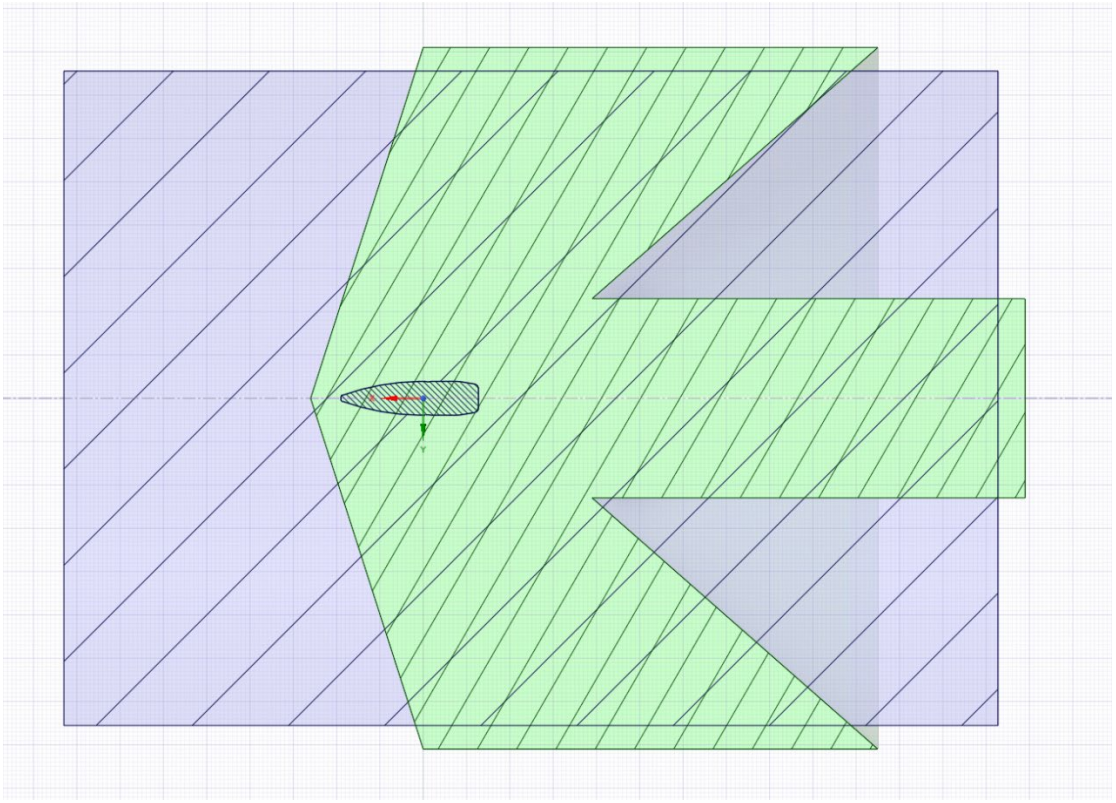

Figure A.2 The wind tunnel geometry. The blue area is a cross section of the cylindrical wind tunnel. A "body of influence" which is used in Ansys Meshing to define a volume with finer mesh is shown in green.

B The radar tracking

The radar used is a doppler radar which emits electromagnetic radiation at frequency of 10.65 GHz (wavelength of 28 mm). The doppler frequency (the difference in frequency between the emitted and received signal) is directly proportional to the radial velocity of the projectile. The digitalized doppler signal is Fourier transformed by a Fast Fourier Transform (FFT) algorithm to determine the peak frequency. A typical FFT window consists of 1024 points (covering 7 ms) with a 50% overlap between each window.

The measured radial velocity history is smoothed and further processed with a point mass model to get the drag coefficient versus Mach number, taking account of parallax and meteorological data (Grandum 2021).

References

ArrowTech Inc (2002): PRODAS V3, www.prodas.com.

Cayzac R., Carette E., Champigny P., Thepot R., Donneaud O., (2004), Analyses of static and dynamic stability of spinning projectiles. 21st International Symposium on Ballistics, Adelaide, Australia, 2004.

Danaberg J.E. and Nietubicz, Predicted flight performance of base-bleed projectiles, Journal of Spacecraft and rockets, Vol. 29, No. 3, May-June 1992.

Dietrich F., Guillen ph., Cayzac R., (2004), Projectile trajectory simulation using CFD code. "21 th Int. Symp. Ballistics, Adelaide, South Australia.

Kubberud N., Øye I.J., (2011), Extended range of 155mm projectile using an improvised base bleed unit: simulations and evaluation. 26th International Symposium on Ballistics, Miami, FL, September 12-16, 2011.

McCoy, R.I., (1985), Aerodynamic and Flight Dynamic Characteristics of the New Family of 5.56 MM NATO Ammunition, BRL Report No. 3467, U.S., Army Ballistic Research Laboratory: Aberdeen Proving Ground, MD.

McCoy, R.I., (1988), The Aerodynamic Characteristics of 7.62mm Match Bullets, BRL Report No. 3733, U.S., Army Ballistic Research Laboratory: Aberdeen Proving Ground, MD.

Sahu J. and Heavey K.R, Computational study of base bleed flow and comparison with experimental data, 16 th International Symposium on Ballistics, San Francisco CA, USA, 23-28 September 1996.

Sharif M.a.R., Guo G., (2007), Computational analysis of supersonic turbulent boundary layers over rough surfaces using the k-omega and stress – omega models. Appl. Math. Model. (31) (12), 2655-2667.

Silton S.I., Weinacht P., (2008), Effect of rifling grooves on the performance of small-caliber ammunition. Technical report, U.S., Army Research Laboratory Aberdeen Proving Ground, MD 21005-5006, Aberdeen Proving Ground, MD, December 2008.

Silton S.I., Howell B.E., (2011), Predicting the dynamic of small-caliber ammunition. 26th International Symposium on Ballistics, MIAMI, FL., 2011.

Simon F., Deck, S., Guillen P., Cayzac R., Sagaut P., Merlen A., (2007), RANS/LES Simulations of projectiles with and without rotations in the subsonic and the transonic regimes, 23rd International Symposium on Ballistics, Tarragona, Spain, 2007.

Suliman M.A., Mahmoud O.K., Al-Sanabawy M.A., Abedel-Hamid O.E., (2009), Computational investigation of base drag deduction for a projectile at different flight regimes.13th International Conference on Aerospace Sciences and Aviation Technology, ASAT-13, May 26-28, 2009.

Zhang C.X.-Z, Kim S.I., Hassan I., (2008), Detached-Eddy simulation of a louver cooling scheme for turbine blades. Journal of Propulsion and Power, Vol. 24, No.5.

Grandum Ø, (2021), Algorithms for analysis of ballistic radar data, FFI-report 21/02284, Norwegian Defence Research Establishment (FFI).

About FFI

The Norwegian Defence Research Establishment (FFI) was founded 11th of April 1946. It is organised as an administrative agency subordinate to the Ministry of Defence.

FFI's mission

FFI is the prime institution responsible for defence related research in Norway. Its principal mission is to carry out research and development to meet the requirements of the Armed Forces. FFI has the role of chief adviser to the political and military leadership. In particular, the institute shall focus on aspects of the development in science and technology that can influence our security policy or defence planning.

FFI's vision

FFI turns knowledge and ideas into an efficient defence.

FFI's characteristics

Creative, daring, broad-minded and responsible.

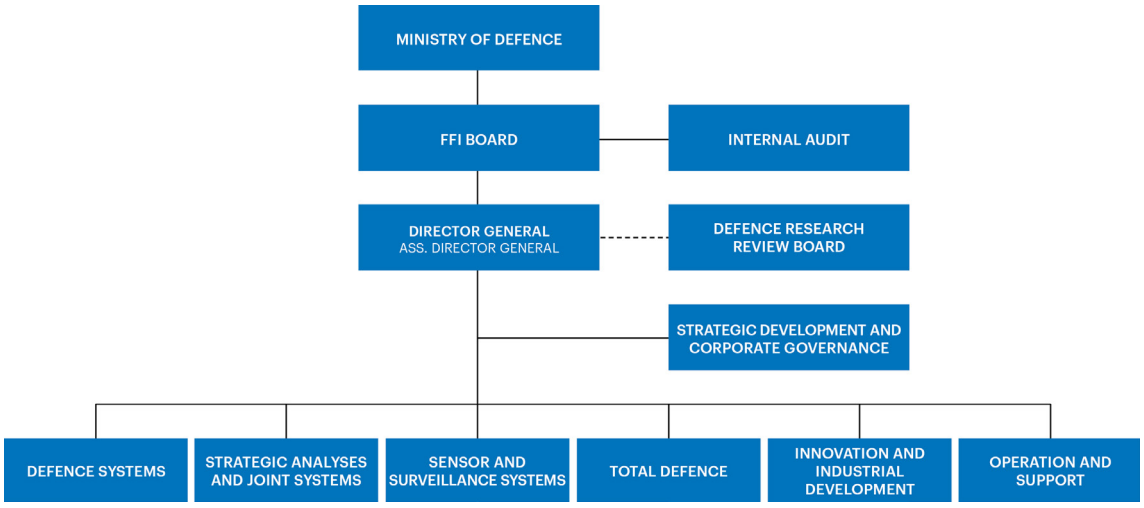

Forsvarets forskningsinstitutt (FFI)
Postboks 25
2027 Kjeller

Besøksadresse:
Kjeller: Instituttveien 20, Kjeller
Horten: Nedre vei 16, Karljohansvern, Horten

Telefon: 91 50 30 03
E-post: post@ffi.no
ffi.no

Norwegian Defence Research Establishment (FFI)
PO box 25
NO-2027 Kjeller
NORWAY

Visitor address:
Kjeller: Instituttveien 20, Kjeller
Horten: Nedre vei 16, Karljohansvern, Horten

Telephone: +47 91 50 30 03
E-mail: post@ffi.no
ffi.no/en